Agricultural and Forest Meteorology 216 (2016) 129–140

Contents lists available at ScienceDirect

Agricultural and Forest Meteorology

journal homepage: www.elsevier.com/locate/agrformet

Soil heat flux calculation for sunlit and shaded surfaces under row crops: 2. Model test☆

Paul D. Colaizzi[a,*], Steven R. Evett[a], Nurit Agam[b], Robert C. Schwartz[a], William P. Kustas[c], Michael H. Cosh[c], Lynn McKee[c]

[a] USDA-ARS Conservation and Production Research Laboratory, Bushland, TX, USA
[b] Blaustein Institutes for Desert Research, Ben-Gurion University of the Negev, Sede-Boqer Campus, 84990, Israel
[c] USDA-ARS Hydrology and Remote Sensing Laboratory, Beltsville, MD, USA

ARTICLE INFO

Article history:
Received 17 September 2014
Received in revised form 5 August 2015
Accepted 11 October 2015

Keywords:
Calorimetric method
Cotton
Energy balance model
Irrigation
Model sensitivity
Texas

ABSTRACT

A method to calculate surface soil heat flux (G_0) as a function of net radiation to the soil ($R_{N,S}$) was developed that accounts for positional variability across a row crop interrow. The method divides the interrow into separate sections, which may be shaded, partially sunlit, or fully sunlit, and calculates $R_{N,S}$ for each interrow section using a relatively simple geometric approach. Normalized $R_{N,S}$ is then related to normalized G_0 for 24 h time steps through a single empirical parameter. The method was tested against G_0 determined using the calorimetric method for upland cotton (*Gossypium hirsutum* L.) with north–south (NS) and east–west (EW) row orientations from sparse to full canopy cover at Bushland, Texas, USA. Data were grouped by canopy cover for three periods in the growing season, including sparse (BEG), medium (MID), and full (END). For each row orientation, measurements used for calorimetric G_0 were located at five interrow positions in two replicates; one position was used for model calibration, and four positions were used for the model test. For NS, soil temperature and volumetric soil water content at 0.02 and 0.06 m depths and soil heat flux at the 0.08 m depth below the surface were measured. For EW, soil temperature and soil heat flux were measured at the same depths and positions as for NS, but volumetric water content was obtained only at a single depth (0.05 m) and in the interrow center in three replicates. Discrepancy between calculated and calorimetric G_0 was larger for EW compared with NS rows for BEG and MID periods (partial canopy cover), but nearly the same during the END period (full canopy cover). During BEG and MID, the greater discrepancy of calorimetric G_0 vs. calculated G_0 for EW rows compared with NS may have been related to measurement of volumetric soil water at only a single depth and interrow position, as well as lower sensor accuracy, compared with those used in NS rows. For NS, the Nash–Sutcliffe modified Index of Agreement was 0.81–0.84; for EW, it was 0.69–0.78 throughout the growing season. The method provided a straightforward way to account for positional variability of G_0 across a row crop interrow, which was most important for NS rows during sparse to medium canopy cover.

Published by Elsevier B.V.

1. Introduction

Surface soil heat flux (G_0) is an important component of the soil–plant–atmosphere energy balance. For bare soil, G_0 can be up to 50% of net radiation (R_N); for partial vegetation cover, particularly row crops, G_0 and soil net radiation ($R_{N,S}$) can have substantial positional variation as related to soil illumination by direct beam solar irradiance (Ham and Kluitenberg, 1993; Heilman et al., 1994;

Abbreviations: a, empirical constant used in surface soil heat flux model (no units); BEG, beginning period of the study during sparse canopy cover; END, end period of the study during full or nearly full canopy cover; EW, east–west crop row orientation; f_{SIS}, fraction of shading of an interrow section (no units); G_0, soil heat flux at the soil surface (W m^{-2}); $G_{0,MAX}$, maximum G_0 over 24 h (midnight to midnight) (W m^{-2}); $G_{0,MIN}$, minimum G_0 over 24 h (midnight to midnight) (W m^{-2}); MID, middle period of the study during intermediate canopy cover; NS, north–south crop row orientation; R_N, total net radiation (W m^{-2}); $R_{N,S}$, soil net radiation (W m^{-2}); $R_{N,S,MAX}$, maximum $R_{N,S}$ over 24 h (midnight to midnight) (W m^{-2}); $R_{N,S,MIN}$, minimum $R_{N,S}$ over 24 h (midnight to midnight) (W m^{-2}).

☆ Mention of company or trade names is for description only and does not imply endorsement by the USDA. The USDA is an equal opportunity provider and employer.

* Corresponding author.
E-mail address: paul.colaizzi@ars.usda.gov (P.D. Colaizzi).

http://dx.doi.org/10.1016/j.agrformet.2015.10.009
0168-1923/Published by Elsevier B.V.

Kustas et al., 2000; Agam et al., 2012a,b; Evett et al., 2012a). In situ estimates of G_0 can be made using the calorimetric or temperature gradient methods, which require measurements of soil heat flux (calorimetric only), soil temperature, and volumetric soil water content at depths down to 0.1–0.2 m below the surface (Sauer and Horton, 2005).

Estimates of G_0 by the calorimetric, temperature gradient, or other methods are limited by the number of in situ measurements that can be practically obtained. Because G_0 is primarily related to R_N or $R_{N,S}$, for practical applications it is typically calculated as a function of these (e.g., Santanello and Friedl, 2003) and sometimes other parameters in order to account for changes in vegetation cover (e.g., Kustas and Daughtry, 1990; Kustas et al., 1993). Most applications consider spatial scales larger than the substrate (soil) and vegetation, and hence do not account for the spatial variation that is known to occur at smaller scales (Maes and Steppe, 2012). Furthermore, the small-scale spatial variability of some energy flux components may tend to cancel out at longer (i.e., daily or 24 h) time steps for row crops even with partial cover; these components include G_0 (Agam et al., 2012a) and soil evaporation (Agam et al., 2012b). On the other hand, many energy balance models are designed to be driven by remotely sensed measurements of surface reflectance and brightness temperature. These applications often rely on one-time-of-day measurements, and therefore must be temporally scaled to daily or longer time steps (Peters and Evett, 2004; Colaizzi et al., 2006; Van Niel et al., 2011, 2012). Errors in any one-time-of-day calculated energy balance component, such as G_0, can potentially lead to larger errors following temporal scaling (Colaizzi et al., 2014). For row crops with partial cover, sources of error might include changes in the proportion of sunlit and shaded soil impacting the overall surface energy balance. Our hypothesis is that soil–plant–atmosphere energy balance models, particularly those designed for remote sensing applications, might be improved by accounting for the positional variation of sunlit and shaded soil beneath a row crop.

Calculation of $R_{N,S}$ to differentiate between shaded, partially sunlit, and fully sunlit soil beneath a row crop is straightforward using a geometric approach. Therefore, Colaizzi et al. (2015) described such a procedure to calculate $R_{N,S}$, and a new approach was also developed to calculate G_0 as a function of $R_{N,S}$ that required only one empirical parameter. The objective of this paper is to test this procedure by comparing calculated G_0 to calorimetric G_0 at different positions across a row crop interrow and for two row orientations.

2. Methods

2.1. Calorimetric and calculated G_0

Brief reviews of calorimetric and calculated (i.e., modeled) G_0 are presented here; additional details are in Colaizzi et al. (2015). The sign convention is positive toward the soil surface, and all fluxes have W m^{-2} units unless otherwise stated. In the calorimetric method, G_0 is the sum of measured heat flux (i.e., by heat flux plates) at depth Zp below the soil surface (G_{Zp}) and divergent heat flux in soil layers between the surface and the plates ($\Delta G_{0,Zp}$):

$$G_0 = G_{Zp} + \Delta G_{0,Zp}, \tag{1}$$

where

$$\Delta G_{0,Zp} = \frac{\sum_{j=1}^{N}(T_{s,zj,i+1} - T_{s,zj,i})\Delta z_j C_{zj}}{(t_{i+1} - t_i)} \tag{2}$$

where j is the soil layer, z_j is the depth of the midpoint of layer j, N is the total number of layers, $T_{s,z}$ is the soil temperature (K) at depth z at successive time steps t_{i+1} and t_i (s), Δz_j is the thickness of soil layer j (m), and C_{zj} is the volumetric heat capacity of the soil in layer j (J m^{-3} K^{-1}), calculated as:

$$C_{zj} = \rho_{M,zj}c_{M,zj}\theta_{M,zj} + \rho_{W,zj}c_{W,zj}\theta_{W,zj} + \rho_{O,zj}c_{O,zj}\theta_{O,zj} \tag{3}$$

where ρ is the density (Mg m^{-3}), c is the specific heat (J kg^{-1} K^{-1}), and θ is the volumetric content (m^3 m^{-3}), and subscripts M, W, and O, stand for minerals, water, and organic constituents, respectively. Volumetric heat capacities were calculated as $\rho_{M,zj}c_{M,zj} = 2.0 \times 10^6$ J m^{-3} K^{-1} and $\rho_{W,zj}c_{W,zj} = 4.2 \times 10^6$ J m^{-3} K^{-1} and assumed constant for each soil layer, and $\theta_{O,zj}$ was negligible (Evett et al., 2012a). Also for each soil layer, $\theta_{M,zj}$ was calculated as $\rho_{b,zj}/\rho_{M,zj}$, where $\rho_{b,zj}$ is soil bulk density and $\rho_{M,zj} = 2.65$ Mg m^{-3}, and $\theta_{W,zj}$ was measured (described in the next section).

A G_0 model based primarily on calculated $R_{N,S}$ was developed by Colaizzi et al. (2015) as:

$$G_0 = \frac{R_{N,S} - R_{N,S,MIN}}{R_{N,S,MAX} - R_{N,S,MIN}}\left(aR_{N,S,MAX} + R_{N,S,MIN}\right) - R_{N,S,MIN} \tag{4}$$

where $R_{N,S,MIN}$ and $R_{N,S,MAX}$ are, respectively, the minimum and maximum $R_{N,S}$ during a 24 h period, and $a = -0.31$. Calculation procedures for $R_{N,S}$ and related terms are in Colaizzi et al. (2012, 2015). It should be noted that measurements were available for R_N but not for $R_{N,S}$. However, Colaizzi et al. (2015) showed that calorimetric G_0 was poorly correlated to R_N but better correlated to $R_{N,S}$ during midday for mid to full canopy cover, which gave stronger justification to develop the model using $R_{N,S}$. This nonetheless imposed a limitation to this study where calculated vs. measured $R_{N,S}$ could not be compared; therefore, the relative impacts of calculated $R_{N,S}$ and assumptions of Eq. (4) could not be assessed in explaining discrepancies between calorimetric and calculated G_0. Although $R_{N,S}$ is inherently more difficult to measure compared to R_N for vegetated surfaces due to numerous factors, future studies should nonetheless strive to improve measurements of this and other relevant variables near the soil surface (Pieri, 2010).

2.2. Field measurements

All field measurements used to evaluate the model were obtained at the USDA Agricultural Research Service Conservation and Production Research Laboratory, Bushland, Texas, USA (35°11′ N lat., −102°06′ W long., 1170 m elevation M.S.L.). The soil is a Pullman clay loam (fine, mixed, super active, thermic torrertic Paleustolls) with slow permeability (USDA-NRCS, 2015), having a dense Bt layer from about 0.3–1.3-m depth and a calcic horizon that begins at approximately the 1.3-m depth. Field measurements were obtained during the Bushland Evapotranspiration and Agricultural Remote sensing EXperiment 2008 (BEAREX08) (Evett et al., 2012b). Details of the field experiment, including measurements of micrometeorology variables (solar irradiance, air temperature, relative humidity, wind speed) and plant samples (width, height, and leaf area) are given in Colaizzi et al. (2015) and in Evett et al. (2012b), but are briefly reviewed here.

Cotton (*Gossypium hirsutum* L.) was seeded on May 17, 2008 on raised beds in four 4.7 ha fields that contain large monolythic weighing lysimeters located in the field centers. The fields are arranged in a square pattern; the east two fields were irrigated by a lateral move sprinkler system, and the west two fields were not irrigated (dryland production). The seed rate in the irrigated fields was 15.8 seeds m^{-2}, and fields were designated northeast (NE) and southeast (SE). The crop was planted in row orientations of north–south (NS) for the NE field, and east–west (EW) for the SE field. Following crop establishment, furrow dikes were installed in the interrows to control run on and runoff of rain and irrigation water (Schneider and Howell, 2000). Micrometeorology variables were measured at the weighing lysimeter site and at a grass reference site immediately east of the SE field, where grass was fully

irrigated by subsurface drip irrigation and maintained at heights between approximately 0.12 and 0.20 m. All data were subject to quality assurance procedures following Allen et al. (1998). Plant height and width were measured approximately weekly at locations throughout the fields, at the lysimeters, and at instrumented sites about 30 m from the NE and SE lysimeters. Destructive plant samples were also obtained during key crop development stages at locations throughout the fields, but away from the lysimeter and other instrumented sites, immediately following height and width measurements. Leaf area was measured on the plant samples, and leaf area index was calculated. Mean values of plant variables were estimated between measurement days by interpolation of cotton growing degree days using a 15.6 °C base temperature.

Estimates of G_0 were obtained by the calorimetric method as described in Colaizzi et al. (2015) (also see Sauer and Horton, 2005, and Evett et al., 2012a for comprehensive reviews of this method). Measurements of soil temperature, volumetric soil water content, and soil heat flux were obtained at instrumented sites approximately 30 m NNE of the NE and SE lysimeters. The instrumented site in the NE field was termed the Primary site, and that in the SE field was termed the Auxiliary site.

In the NE field, soil temperature was measured by thermocouples that were constructed in-house of Type T (copper constantan) wire (model EXPP-T-20-TWSH wire, Omega Engineering, Inc., Stamford, CT) (Evett et al., 2012a). Volumetric soil water content was measured using time-domain reflectometry (TDR) trifilar probes. The probes, multiplexors, TDR instrument, and TDR waveform interpretation algorithm comprise a complete system described by Evett (2000a,b) and Evett et al. (2005, 2012a), and were calibrated to the Pullman clay loam soil, resulting in root mean square error (RMSE) $\leq$0.01 m^3 m^{-3} (Evett et al., 2005). The thermocouples and TDR probes relevant to this study were installed horizontally at the 0.02 m and 0.06 m depths below the surface, and at five positions spaced 0.15 m apart across the crop interrow (Fig. 1a). Each position was replicated twice, resulting in a total of ten positions numbered according to Fig. 1b. Soil heat flux at the 0.08-m depth was measured by soil heat flux plate flow transducers (model HFT-3.1, Radiation and Energy Balance Systems, Inc., Bellevue, WA); these were at the same ten positions as the thermocouple and TDR probes (Fig. 1a). Soil heat flux divergence above the soil heat flux plates was calculated for two soil layers, from 0 to 0.04 m and from 0.04 to 0.08 m, where the thermocouples and TDR probes were in the center depths (0.02 and 0.06 m) of these layers.

In the SE field, thermocouples and soil heat flux plates consisted of the same model and manufacturer, and were deployed at the same depths and positions relative to the crop rows as the NE field, except row orientation was EW (Fig. 1c). Volumetric soil water was measured by capacitance probes (model Hydra Probe, Stevens Water Monitoring Systems, Inc., Portland, OR). The capacitance probes were installed horizontally at the 0.05-m depth at three locations along the center of the interrow; the probes sensed a depth from 0.03 to 0.07 m (Cosh et al., 2012). Volumetric soil water contents measured by the three probes were averaged, resulting in a single value for all locations and depths in the SE field site. Nonetheless, soil heat flux divergence was calculated for two soil layers in the same manner as for the NE field because soil temperature was measured at the 0.02 and 0.06 m depths. The capacitance probes were calibrated to the TDR probes using six additional capacitance probes deployed in the NE field near the TDR probes, resulting in RMSE ~0.03 m^3 m^{-3} (Agam et al., 2012a).

The model was tested using measurements at each position except for positions 3a and 3b in the NE field; data from those positions were used in Colaizzi et al. (2015) to find the empirical coefficient. Ten measurement days were selected from three crop growth periods during the season in order to evaluate the model under a wide range of canopy cover, and also to be consistent with Colaizzi et al. (2015) and previous studies of these data (Agam et al., 2012a; Evett et al., 2012a). These periods were termed the beginning (BEG), middle (MID), and ending (END). Each period included days of year (DOY) 181–184, 186–189, and 193–194 for BEG; 205–206, 208–209, 211, 213, 215, 217, 219, 222 for MID; and 239–241, 244–245, 248–251, and 254 for END. Each measurement day included 30-min averages of data, and excluded irrigation events.

2.3. Model comparison using interrow-averages and interrow sections

Calculated vs. calorimetric G_0 was compared in three ways. First, the interrow-average of $R_{N,S}$ and hence G_0 were calculated and compared with the interrow average of calorimetric G_0. Second, the interrow-average of calculated G_0 was compared to calorimetric G_0, where calorimetric G_0 was estimated separately for nighttime, shaded, partially sunlit, and completely sunlit surface conditions. Here, during the daytime and for each 30-min interval, each interrow section was classified as being shaded, partially shaded, or fully sunlit, and interrow sections were averaged that had the same classification. Third, both calculated and calorimetric G_0 were separated into the different surface conditions as before and compared. Although interrow sections could be classified as "shaded," it should be noted that sun flecks may nonetheless be present from transmittance of direct bean shortwave irradiance through the canopy (see equations 7a and 7c in Colaizzi et al., 2015). Model evaluation in these three ways was done to assess the justification for considering positional variation across the interrow.

Calculation of the interrow-average of $R_{N,S}$ (and hence G_0) required changing only two variables in the $R_{N,S}$ model (equations 5–11 in Colaizzi et al., 2015). The first variable was the fraction of shading of an interrow section (f_{SIS}), which is used to calculate the shortwave direct beam components (equations 7a and 7c in Colaizzi et al., 2015). This was replaced by the solar canopy view factor (f_{SC}; see Colaizzi et al., 2012, Appendix 2 for the calculation procedure). The second variable was the hemispherical view factor of the canopy (f_{HC}), which is used to calculate the shortwave diffuse (equations 7b and 7d in Colaizzi et al., 2015) and longwave components (equation 8 of Colaizzi et al., 2015). This was calculated for a single position 2 m directly above the crop row, instead for each of the five interrow measurement positions. With the interrow-average $R_{N,S}$ calculated, the interrow-average G_0 was then calculated using Eq. (4).

2.4. Model evaluation statistics

The discrepancy between calculated and calorimetric G_0 was quantified following the recommendations of Legates and McCabe (1999), where statistical parameters reported included the average and standard deviation (SD) of calculated and calorimetric G_0 samples, index of model agreement (IOA), root mean square error (RMSE), mean absolute error (MAE), and mean bias error (MBE). The IOA is essentially a non-squared version of the Nash and Sutcliffe (1970) model efficiency parameter, which is recommended due to its decreased sensitivity to outliers compared with higher orders. Similar to the Nash–Sutcliffe parameter, the IOA can range from $-\infty$ to 1.0, where IOA = 1.0 indicates perfect model agreement, and IOA = 0 indicates the model is no better than the sample mean of all measurements. Although RMSE and MAE can include both systematic and unsystematic error, systematic error may also be assessed through MBE. RMSE will always be greater than MAE, and the greater discrepancy between the two indicates greater presence of outliers in the data.

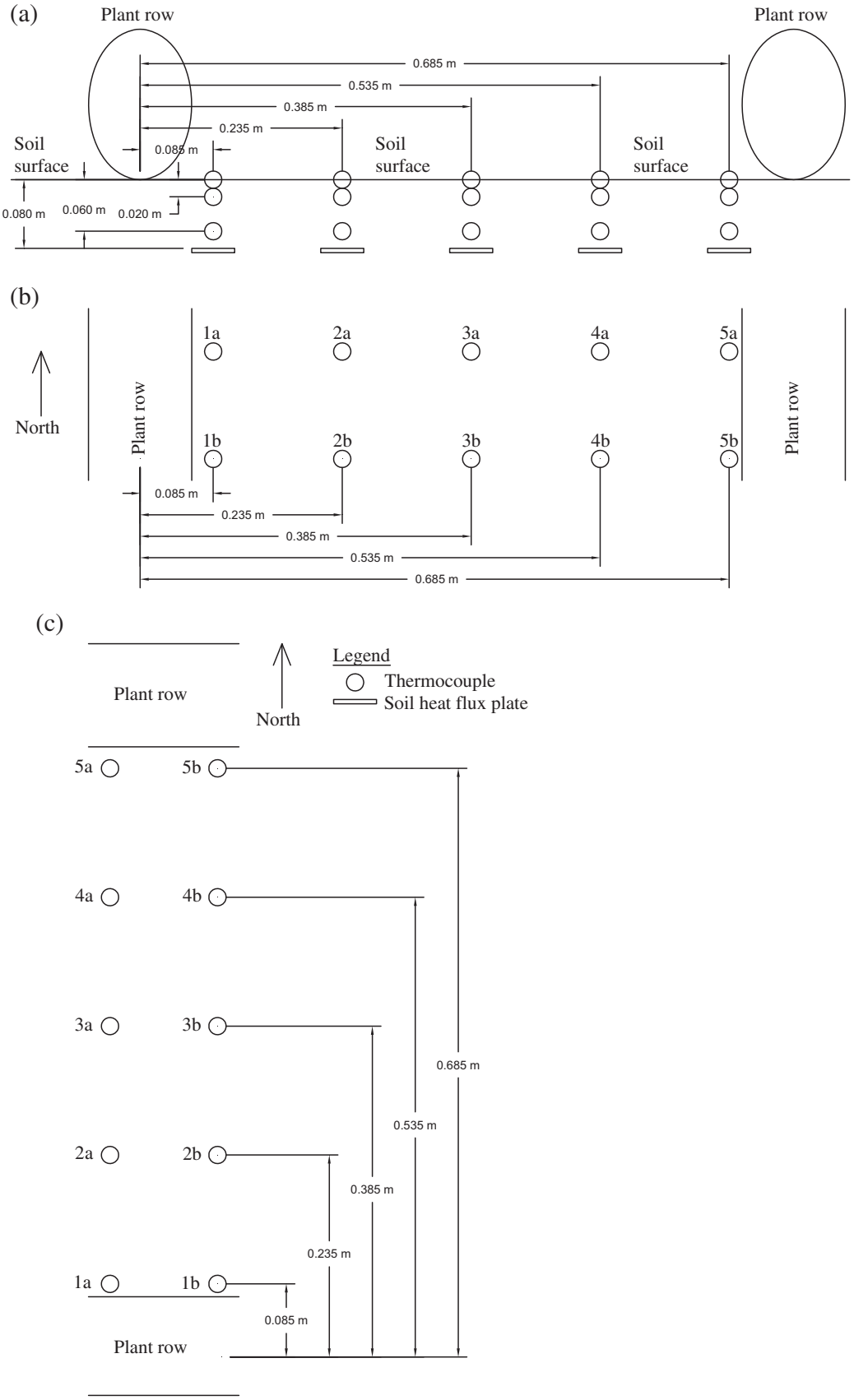

Fig. 1. Measurement positions of thermocouples and soil heat flux plates relative to plant rows; (a) side view; (b) top view for north–south (NS) rows; (c) top view for east–west (EW) rows.

3. Results and discussion

3.1. Plant temporal and spatial variability

The model was evaluated for a wide range of canopy cover with spatial variability that might be expected in commercial agricultural fields. Cotton growth and development were delayed up to around the start of the BEG period due to very hot and windy conditions, but developed at near normal rates thereafter because growing conditions were more favorable. From the BEG to MID periods, both the NE and SE fields exhibited increasing spatial variability of canopy width, canopy height, and leaf area index; spatial variability decreased somewhat in the NE field and remained about the same in the SE field from the MID to END periods (Fig. 2). During the MID and early END periods, spatial variability was greater in the NE field compared with the SE, and plants developed more rapidly in the NE lysimeter and Primary site locations compared with other NE field locations.

Leaf area measurements were obtained only at locations away from instrumented sites where plants may not have developed as rapidly. Although this would imply that leaf area index was greater at the Primary site compared with the field-averaged value during this time, the field-averaged leaf area index was nonetheless used in $R_{N,S}$ calculations, and no attempt was made to adjust this because the correlation between leaf area index and plant height was judged inadequate to justify this. Therefore, at least some discrepancy between calculated and calorimetric G_0 may have been due to underestimates of leaf area index. From the sensitivity analysis in Colaizzi et al. (2015), sensitivity to leaf area index was largest during the MID and END periods for shaded and partially sunlit soil, and NS rows usually had greater sensitivity compared with EW rows.

In both the NE and SE fields, full canopy cover was reached at approximately DOY 226 (between MID and END periods), when plant width reached ~0.76 m, which is the row spacing. However, plants did not reach maximum height until around DOY 260, after the END period. In the NE field, maximum leaf area index was reached between DOY 220 and 240, and around DOY 240 for the SE field. Unfortunately, plant width and height measurements were obtained too infrequently at the Auxiliary site, although this may have been less consequential because plants developed more uniformly and spatial variability was less in the SE field.

3.2. Interrow-averaged calculated G_0 vs. interrow-averaged calorimetric G_0

The sign convention for all energy flux terms used herein is positive toward the surface. Therefore, maximum and minimum G_0 occur at night and day, respectively. The maximum magnitude of G_0 occurred during the day in all cases. The range of calorimetric and calculated G_0 was largest during the BEG, intermediate during the MID period, and smallest during the END period, as expected (Fig. 3, Table 1). Although the NE field had greater spatial variability (and uncertainty in leaf area index), and although the model generally had greater sensitivity to NS rows (NE field) compared with EW rows (SE field), agreement between calculated and calorimetric G_0 was closer for the NE field compared with the SE field for all three periods. This is indicated by the larger IOA and smaller RMSE, MAE, and MBE (Table 1), and less visible scatter (Fig. 3). The differences in model agreement for these fields is most likely related to differences in measurement accuracy and measurement positions of volumetric soil water content, which is required to calculate the volumetric heat capacity of the soil and hence heat flux divergence in soil layers above the soil heat flux plates.

In both fields, the magnitude of MBE (|MBE|) was largest during the BEG period, especially when calorimetric $G_0 < 0$ during the daytime, but smallest during the END period (Fig. 3, Table 1). This indicated that during the BEG period, the model tended to overestimate the magnitude of daytime values of G_0 ($|G_{0,DAY}|$). A number of factors could contribute to this, such as leaf area index, the (a) empirical parameter used in the $G_{0,MIN} = a \times R_{N,S,MAX}$ assumption, and the $G_{0,MAX} = -R_{N,S,MIN}$ assumption, as described in Colaizzi et al. (2015), or error in $R_{N,S}$ calculation. However, comparison of model results between the BEG, MID, and END periods did not consistently support any one factor as an explanation.

An underestimate of leaf area index would directly result in overestimates of $R_{N,S}$ and hence overestimates of $|G_{0,DAY}|$. However, canopy cover was relatively sparse during the BEG period, resulting in the model being insensitive to leaf area index (except for shaded surfaces with NS rows; see Table 2 in Colaizzi et al., 2015), and |MBE| was greater for EW compared with NS rows. Therefore, errors in leaf area index were more likely to increase |MBE| during the MID and END compared with the BEG period, and more so for NS compared with EW rows.

In the present model development, it was assumed that $G_{0,MIN} = a \times R_{N,S,MAX}$, meaning that $G_{0,MIN}$ and $R_{N,S,MAX}$ coincide, and it was also assumed that $a = -0.31$ remained constant throughout the season in order to minimize the dependence on empirical parameters. However, $a = -0.20$ for four of the ten days during the BEG period (Fig. 5b, Colaizzi et al., 2015), which may be a consequence of $G_{0,MIN}$ and $R_{N,S,MAX}$ not coinciding (Fig. 4, Colaizzi et al., 2015) and could have been caused by substantial energy diversion into evaporative flux. Model sensitivity and inspection of Eq. (4) indicate that calculated G_0 is most sensitive to (a) during the daytime (i.e., when $G_0 < 0$), and usually (but not always) for NS compared with EW rows, and for increasing canopy cover. Also, inspection of Eq. (4) indicates that reduction in (a) reduces $|G_0|$ when $G_0 < 0$. Although a reduction of (a) would reduce |MBE| during the BEG period, it would increase |MBE| during the MID and END periods. Also, $G_{0,MIN}$ and $R_{N,S,MAX}$ appeared to coincide more frequently during the BEG period (under sparse canopy cover) compared with the MID and END periods (Fig. 4, Colaizzi et al., 2015), which could lead to poorer model performance as the season progressed and canopy cover increased. However, there were no large differences in IOA between periods. Although RMSE, MAE, and |MBE| were always less for the MID and END periods compared with the BEG period, this could also result from a smaller G_0 range for subsequent periods. Therefore, the relatively large |MBE| during the BEG period could sometimes be explained by (a) overestimates.

Also in the present model development, it was assumed that $G_{0,MAX} = -R_{N,S,MIN}$, meaning that these are assumed to coincide, and that net turbulent heat fluxes at the soil surface were assumed negligible during the nighttime when $G_{0,MAX}$ and $R_{N,S,MIN}$ are most likely to occur. The assumption of $G_{0,MAX}$ and $-R_{N,S,MIN}$ coinciding is not likely to contribute to as large error compared with $G_{0,MIN}$ and $R_{N,S,MAX}$ not coinciding. During the nighttime, G_0 and $R_{N,S,MIN}$ have much less temporal variability compared with daytime values. Therefore, nighttime errors were more likely to be caused by non-negligible net turbulent heat flux. If these are negative (away from the surface, where soil is cooling and evaporation is taking place), then $G_{0,MAX}$ would be underestimated. The positive net turbulent flux scenario, where $G_{0,MAX}$ is overestimated, is also possible, implying soil warming, less rapid soil cooling, and/or condensation (Tolk et al., 2006). With $G_{0,MAX}$ underestimated, calculated G_0 is also underestimated, although this may not be immediately apparent from inspection of Eq. (4). However, calculated G_0 is more sensitive to underestimates of $G_{0,MAX}$ during the nighttime (when $R_{N,S}$ is closer to $R_{N,S,MIN}$) compared with daytime (when $R_{N,S}$ is closer to $R_{N,S,MAX}$). This may explain the slight underestimates of calculated G_0 when calorimetric $G_0 > 0$, which are visible in scatter plots during the BEG and MID periods (Fig. 3).

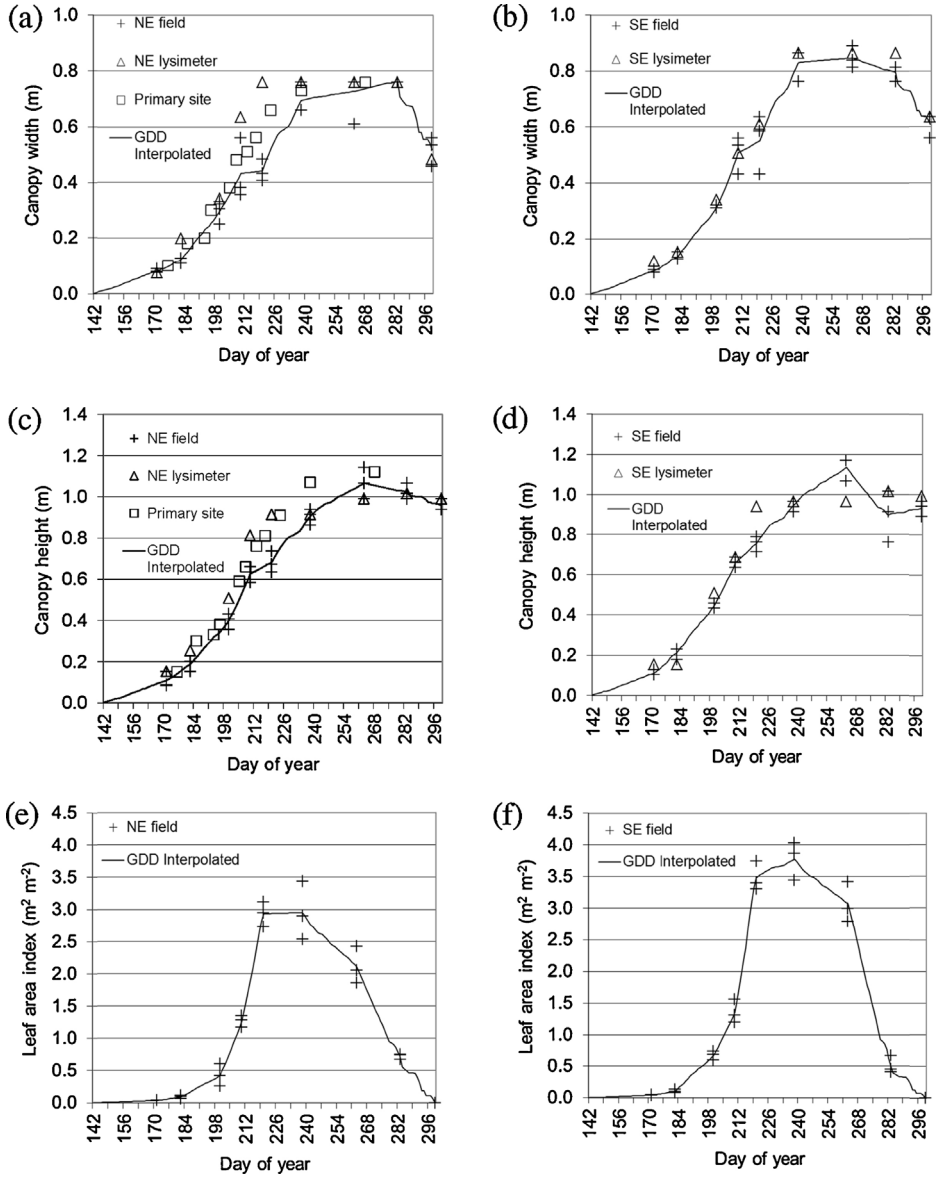

Fig. 2. The 2008 cotton season with measurements of canopy width at (a) NE field (north–south rows); (b) SE field (east–west rows); canopy height at (c) NE field (north–south rows); (d) SE field (east–west rows); leaf area index at (e) NE field (north–south rows); (f) SE field (east–west rows); and linear interpolation between field-averaged measurement days based on growing degree days (GDD Interpolated).

3.3. *Interrow-averaged calculated* G_0 *vs. interrow section calorimetric* G_0

Calorimetric G_0 was partitioned into its nighttime, shaded, partially sunlit, and fully sunlit interrow sections and compared with calculated G_0 that was averaged over the interrow (Table 2, Fig. 4). In contrast to when calorimetric G_0 was averaged over the interrow (Table 1, Fig. 3), the discrepancies between calculated and calorimetric G_0 were much larger for NS compared with EW rows. In addition, the partitioning of calorimetric G_0 resulted in IOA decreasing and RMES, MAE, and |MBE| increasing in all cases except for EW rows during the END period. The |MBE| patterns were similar to those for interrow averaged calorimetric G_0. In a preliminary analysis, horizontal heat flux between positions was also considered in determining calorimetric G_0. This was done using the thermal gradient method described in Evett et al. (2012a), because conduction was assumed the primary driver of horizontal heat transfer near the surface. In this method, horizontal surface G_0 was calculated and added to calorimetric G_0. However, inclusion of horizontal surface G_0 had little impact (<1%) on calorimetric G_0, and hence little impact on model discrepancies (data not shown). This may have been related to vertical temperature and soil water gradients being relatively larger compared with horizontal gradients.

During the BEG period, calculated $|G_{0,DAY}|$ tended to be overestimated relative to calorimetric $|G_{0,DAY}|$, possibly due to (*a*) overestimates and $G_{0,MAX}$ underestimates as described previously. This included partially sunlit surfaces for both NS and EW rows, but NS rows tended to also have a greater proportion of shaded surfaces, whereas EW had a greater proportion of sunlit surfaces. This would be expected because during the summer growing season, the solar azimuth angle is parallel to and illuminates NS interrows once per day (around solar noon), but this occurs twice per day for EW interrows (morning and afternoon).

During the MID period, calculated $|G_{0,DAY}|$ tended to be underestimated for sunlit surfaces and overestimated for shaded surfaces, especially for NS rows (Fig. 3). The largest discrepancy between calculated and calorimetric G_0 occurred for the NS rows with

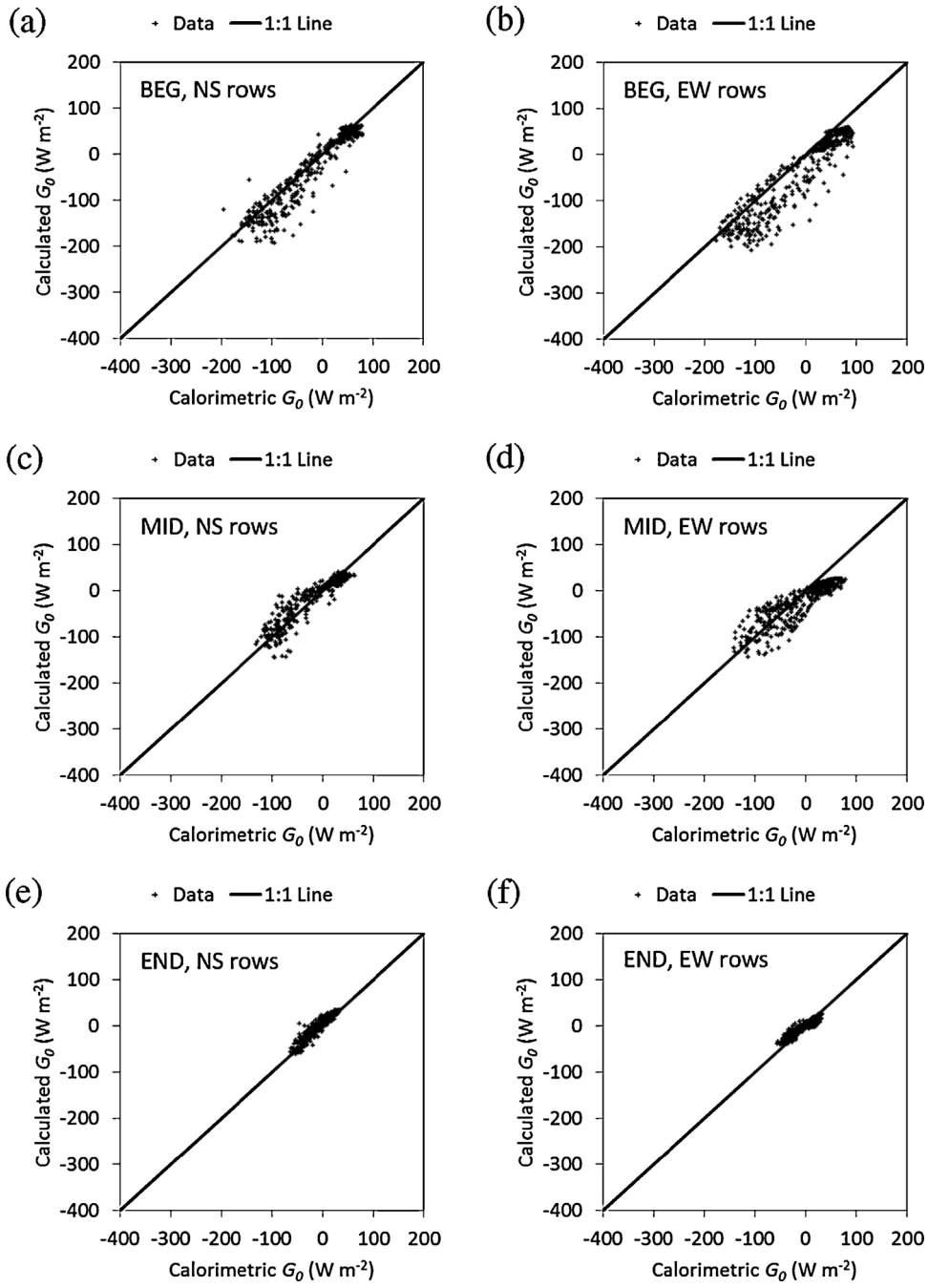

Fig. 3. Scatter plots of calculated vs. calorimetric surface soil heat flux (G_0) for (a) BEG north–south (NS) rows; (b) BEG east–west (EW) rows; (c) MID north–south (NS) rows; (d) MID east–west (EW) rows; (e) END north–south (NS) rows; (f) END east–west (EW) rows, where calculated and calorimetric G_0 were averaged across the interrow. See Table 1 for calculated vs. calorimetric G_0 statistical parameters.

sunlit surfaces, where calculated $|G_{0,DAY}|$ was much less compared with calorimetric $|G_{0,DAY}|$. Since calculated G_0 was averaged across the interrows, most interrow sections included shaded and partially shaded interrow sections, meaning that calculated G_0 was weighted toward smaller values compared with calorimetric G_0 for sunlit interrow sections. During this period, canopy width was 0.36–0.48 m; hence the fraction of canopy cover was 0.47–0.63, and each interrow section was sunlit for 1–2 h once per day. A similar but opposite process likely occurred when interrow sections were shaded, but calculated G_0 also included partially and fully sunlit interrow sections, meaning that calculated G_0 was weighted toward larger values compared with calorimetric G_0 for shaded interrow sections. A similar pattern occurred for EW rows, but calculated and calorimetric discrepancies were less compared with NS rows. This would be expected because changes in $R_{N,S}$ and hence G_0 were less abrupt for EW compared with NS rows for the range of canopy cover during the MID period; this was related to differences in the magnitude and patterns of solar illumination for the two interrow orientations.

During the END period, canopy cover was nearly complete for the NS rows (fraction of cover was 0.92–0.95), and it was complete for the EW rows (fraction of cover was 1.0). A few partially shaded interrow sections occurred at NS rows during the daytime, but nearly all EW interrow sections were shaded except for ten that were partially shaded (Table 2, Fig. 3). Interrow-averaged calculated $|G_{0,DAY}|$ tended to be less than calorimetric $|G_{0,DAY}|$ for

Table 1
Statistical parameters of agreement for calculated vs. calorimetric surface soil heat flux (G_0) averaged across the interrow. See Fig. 3 for scatter plots.

Row dir.[a]	Period	n	Calor. G_0		Calc. G_0		IOA[c]	RMSE[d]	MAE[e]	MBE[f]
			Avg. ($W m^{-2}$)	SD[b] ($W m^{-2}$)	Avg. ($W m^{-2}$)	SD[b] ($W m^{-2}$)		($W m^{-2}$)	($W m^{-2}$)	($W m^{-2}$)
NS	BEG	480	−9.5	70.6	−21.0	77.6	0.87	26.0	16.8	−11.6
NS	MID	480	−3.7	49.4	−4.2	45.2	0.83	18.0	13.0	−0.6
NS	END	480	−0.9	22.7	5.1	22.3	0.81	9.6	7.5	6.0
EW	BEG	480	−7.9	75.0	−36.2	80.2	0.77	40.2	30.8	−28.2
EW	MID	480	−2.8	54.3	−20.4	42.1	0.66	30.7	26.8	−17.6
EW	END	480	−0.5	22.1	−1.8	16.0	0.76	9.4	7.6	−1.3

[a] North–south (NS) and east–west (EW).
[b] Standard deviation.
[c] Index of agreement.
[d] Root mean square error.
[e] Mean absolute error.
[f] Mean bias error.

Table 2
Statistical parameters of agreement for calculated vs. calorimetric surface soil heat flux (G_0), where calculated G_0 was averaged across the interrow, but calorimetric G_0 was separated into day and night, and daytime positions across the interrow. See Fig. 4 for scatter plots.

Row dir.[a]	Period	n	Calor. G_0		Calc. G_0		IOA[c]	RMSE[d]	MAE[e]	MBE[f]
			Avg. ($W m^{-2}$)	SD[b] ($W m^{-2}$)	Avg. ($W m^{-2}$)	SD[b] ($W m^{-2}$)		($W m^{-2}$)	($W m^{-2}$)	($W m^{-2}$)
NS	BEG	819	−34.2	69.3	−49.4	76.6	0.82	35.0	23.2	−15.2
NS	MID	691	−35.3	79.3	−26.4	53.7	0.69	54.1	35.6	8.8
NS	END	520	−5.2	27.2	−1.8	25.6	0.76	13.8	10.5	3.4
EW	BEG	818	−23.3	74.0	−55.5	80.0	0.75	45.0	34.4	−32.1
EW	MID	780	−24.9	63.2	−34.5	44.0	0.66	38.3	30.8	−9.6
EW	END	490	−0.3	21.3	−1.7	15.8	0.77	8.9	7.1	−1.4

[a] North–south (NS) and east–west (EW).
[b] Standard deviation.
[c] Index of agreement.
[d] Root mean square error.
[e] Mean absolute error.
[f] Mean bias error.

the partially sunlit NS interrow sections. As before during the MID period, this likely resulted from interrow-averaged calculated G_0 being weighted toward shaded interrow sections, where resulting calculated $|G_{0,DAY}|$ was less compared with calorimetric $|G_{0,DAY}|$ for partially sunlit interrow sections. For the EW rows, agreement between interrow-averaged calculated G_0 and interrow section calorimetric G_0 (Table 2) was nearly the same as for interrow-averaged calculated and calorimetric G_0 (Table 1), which was expected because all interrow sections were shaded and hence would not have very large positional variation.

3.4. *Interrow section calculated* G_0 *vs. interrow section calorimetric* G_0

Discrepancies between calculated and calorimetric G_0 for each interrow section showed very similar patterns as those for when calculated G_0 was averaged across the interrow (Table 3, Fig. 5). However, discrepancies were much less for NS rows compared with EW rows. During the BEG period, |MBE| was larger for both NS and EW rows compared with the MID and END periods, and calculated $|G_{0,DAY}|$ tended to be greater than calorimetric $|G_{0,DAY}|$ for shaded, partially sunlit, and fully sunlit interrow sections. From the previous discussion, it appears that the most effective refinement to the model approach may be in refining the $G_{0,MIN}$ and $R_{N,S,MAX}$ relationship and the daytime normalized G_0 and $R_{N,S}$ assumption, particularly during small canopy cover.

For NS rows during the BEG and END periods, discrepancies between calculated and calorimetric G_0 were only reduced marginally compared with interrow-averaged calculated G_0 vs. interrow section calorimetric G_0, but there was a substantial reduction in discrepancies during the MID period, particularly for the shaded and fully sunlit interrow sections. The G_0 at these interrow sections would be expected to deviate more from interrow-averaged G_0 compared with G_0 at partially sunlit interrow sections.

For EW rows during the BEG and MID periods, discrepancies between calculated and calorimetric G_0 actually increased marginally when canopy cover was partial, but were nearly the same during the END period when canopy cover was full. However, the positional and depth variability of volumetric soil water was not measured at the Auxiliary site for the EW rows (Cosh et al., 2012). This should have reduced the accuracy of calorimetric G_0 through the volumetric soil heat capacity term and the accuracy of hence heat flux divergence in soil layers above the soil heat flux plates (Agam et al., 2012a). In addition, positional variability across the interrow could potentially be underestimated, especially for partial canopy cover (BEG and MID periods).

These results suggest that accounting for the positional variability of G_0 across interrows is most justified for NS rows during low- to mid-range values of canopy cover (i.e., BEG and MID periods). Positional variability is also important for EW rows, but at different times of the day (Evett et al., 2012a). The greater discrepancy between calculated and calorimetric G_0 for EW compared with NS rows also highlights the importance of striving for the most accurate measurements of volumetric soil water possible, and to deploy a sufficient number of sensors to capture the positional and depth variability that likely exists (Kustas et al., 2000). The overall discrepancies of calculated vs. calorimetric G_0 for interrow sections (Table 3, Fig. 5) were greater compared with discrepancies of calculated vs. calorimetric G_0 averaged across the interrow. This was related to the dataset for individual interrow sections being much larger than interrow-averages, and greater uncertainty of shading and solar illumination (i.e., the f_{SIS} term) for interrow sections. The

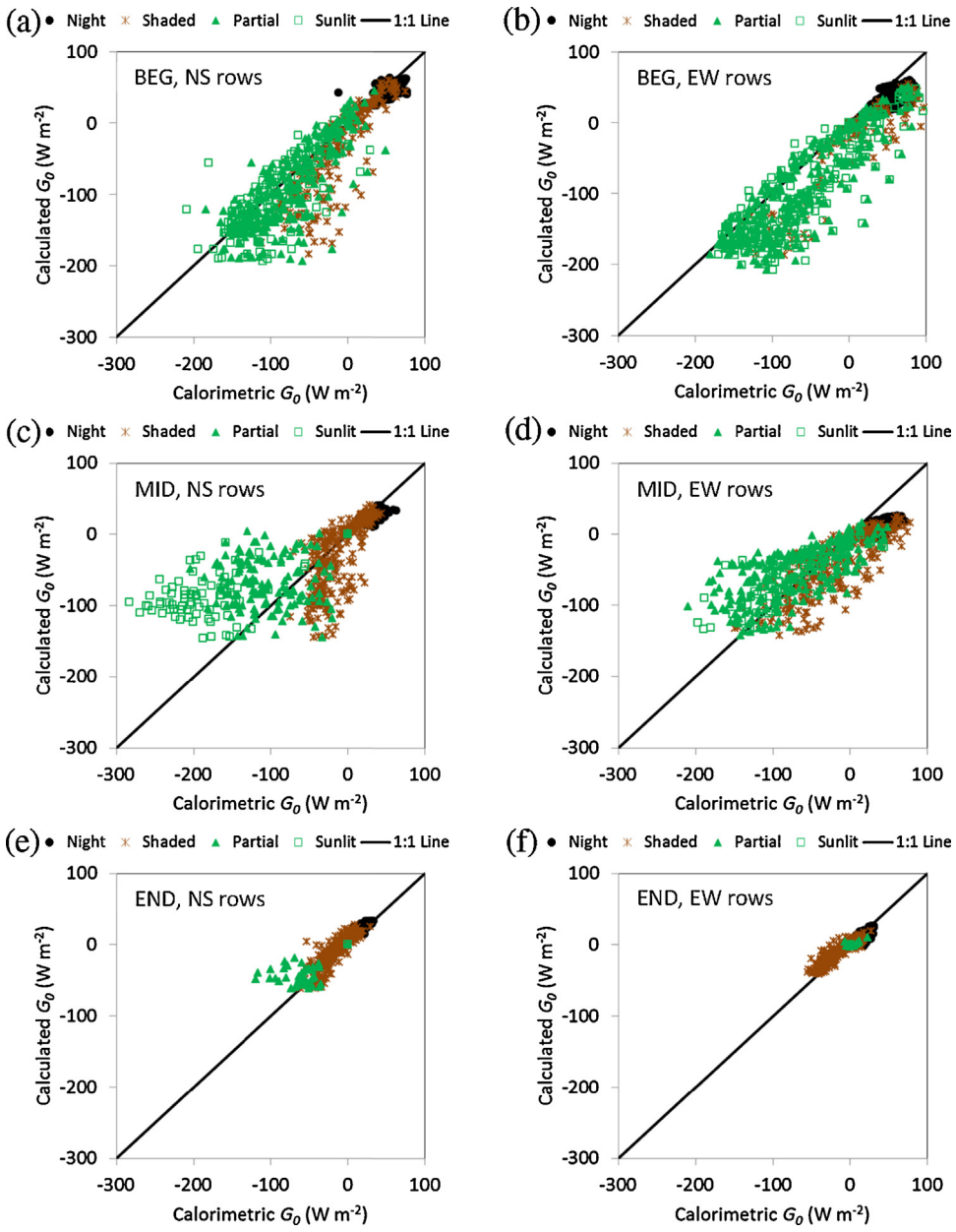

Fig. 4. Scatter plots of calculated vs. calorimetric surface soil heat flux (G_0) for (a) BEG north–south (NS) rows; (b) BEG east–west (EW) rows; (c) MID north–south (NS) rows; (d) MID east–west (EW) rows; (e) END north–south (NS) rows; (f) END east–west (EW) rows, where calculated G_0 was averaged across the interrow, but calorimetric G_0 was separated into day and night, and daytime was partitioned into shaded, partially sunlit, and fully sunlit positions across the interrow. See Table 2 for calculated vs. calorimetric G_0 statistical parameters.

Table 3
Statistical parameters of agreement for calculated vs. calorimetric surface soil heat flux (G_0), where calculated and calorimetric G_0 were separated into day and night, and daytime positions across the interrow. See Fig. 5 for scatter plots.

Row dir.[a]	Period	n	Calor. G_0		Calc. G_0		IOA[c]	RMSE[d]	MAE[e]	MBE[f]
			Avg. (W m^{-2})	SD[b] (W m^{-2})	Avg. (W m^{-2})	SD[b] (W m^{-2})		(W m^{-2})	(W m^{-2})	(W m^{-2})
NS	BEG	819	−34.2	69.3	−48.6	76.3	0.84	31.3	20.6	−14.4
NS	MID	691	−35.3	79.3	−29.2	64.8	0.80	34.8	23.4	6.1
NS	END	520	−5.2	27.2	0.4	28.2	0.81	13.2	9.0	5.6
EW	BEG	818	−23.3	74.0	−53.1	82.1	0.73	49.7	37.3	−29.8
EW	MID	780	−24.9	63.2	−41.0	58.6	0.69	39.1	31.3	−16.1
EW	END	490	−0.3	21.3	−1.3	16.7	0.78	8.8	7.0	−0.9

[a] North–south (NS) and east–west (EW).
[b] Standard deviation.
[c] Index of agreement.
[d] Root mean square error.
[e] Mean absolute error.
[f] Mean bias error.

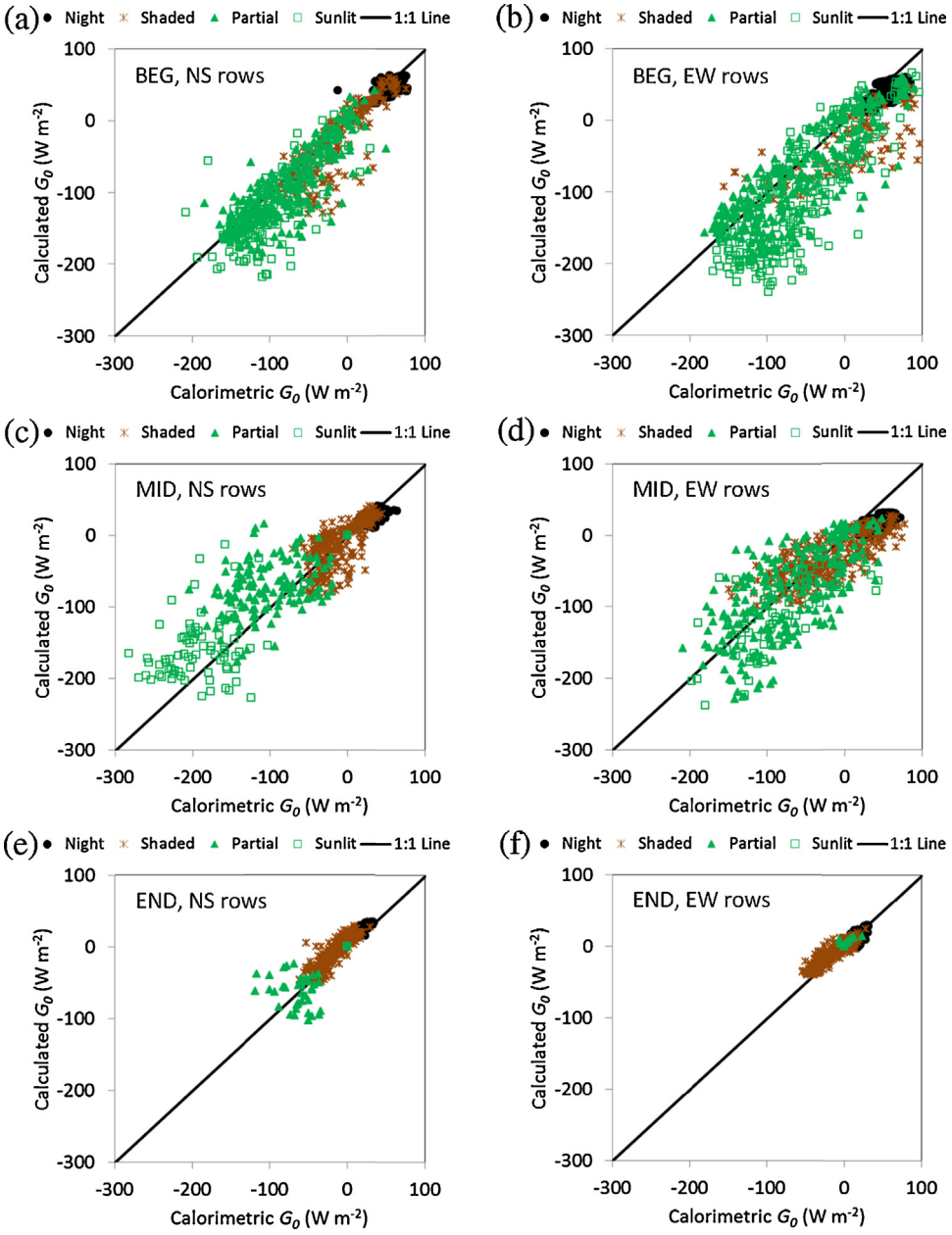

Fig. 5. Scatter plots of calculated vs. calorimetric surface soil heat flux (G_0) for (a) BEG north–south (NS) rows; (b) BEG east–west (EW) rows; (c) MID north–south (NS) rows; (d) MID east–west (EW) rows; (e) END north–south (NS) rows; (f) END east–west (EW) rows, where calculated and calorimetric G_0 were separated into day and night, and daytime was partitioned into shaded, partially sunlit, and fully sunlit positions across the interrow. See Table 3 for calculated vs. calorimetric G_0 statistical parameters.

approach proposed herein provides a straightforward method to account for the positional variability of $R_{N,S}$ and G_0 across a crop interrow.

3.5. *Effect of canopy cover, row orientation, and interrow position on daytime* $R_{N,S} + G_0$

The effect of canopy cover, row orientation, and interrow position on daytime total (sunrise to sunset) available energy to the soil ($R_{N,S} + G_0$) was compared (Fig. 6). Here, daytime total ($R_{N,S} + G_0$) was calculated for each of the five interrow sections and NS and EW row orientations, and averaged during the BEG, MID, and END periods. A similar comparison for calorimetric G_0 was conducted by Agam et al. (2012a). During the BEG period, daytime total ($R_{N,S} + G_0$) was larger for the EW row orientation compared with the NS row orientation for interrow positions 2, 3, 4 and for the interrow average. This resulted because daytime total $R_{N,S}$ was dominated by net shortwave radiation to the soil ($S_{N,S}$), and for EW interrows, the solar and interrow azimuth angles were parallel twice per day, during mid-morning and mid-afternoon. However, for NS interrows, the solar and interrow azimuth angles were parallel only once per day, around solar noon (see also Fig. A.1 in Colaizzi et al., 2015). This was offset by greater soil shading of EW interrows only for positions 1 and 5. A similar pattern would have been expected during the MID period; however, by the MID period the canopy was larger (i.e., greater width, height, and LAI) for EW compared with NS rows (Fig. 2). Therefore, daytime total ($R_{N,S} + G_0$) for NS interrows was larger for all interrow positions except 3 and 4. For both row orientations during the BEG and MID periods, daytime total ($R_{N,S} + G_0$) was larger for interrow positions further away from the crop rows compared with 1 and 5. During the END period when nearly full canopy cover was reached, interrow position had little

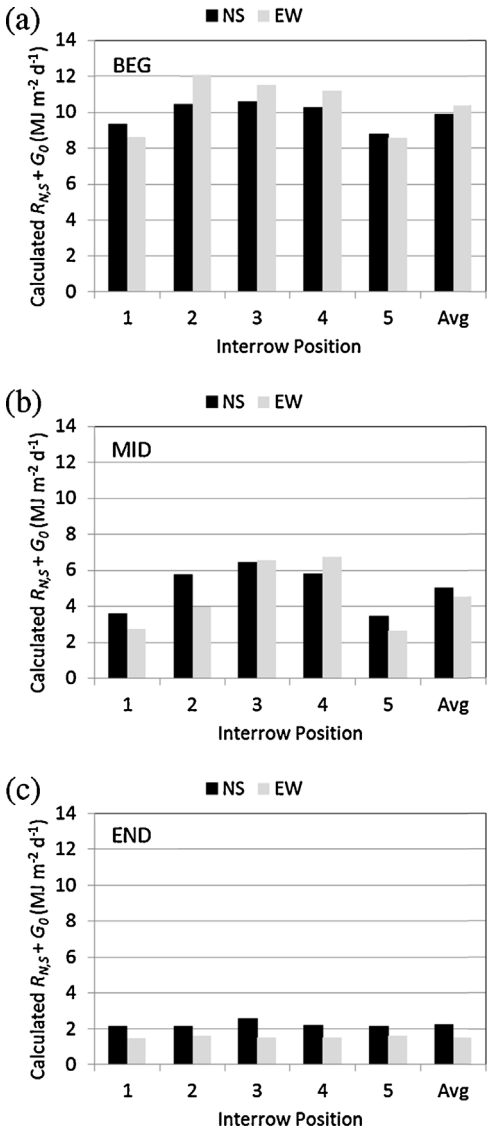

Fig. 6. Calculated daytime total available energy ($R_{N,S}+G_0$) and averaged for (a) BEG; (b) MID; and (c) END periods, each for north–south (NS) and east–west (EW) rows.

influence on daily total ($R_{N,S}+G_0$),and NS was larger than EW rows for all interrow positions because LAI was larger for EW rows. In the present study, differences in canopy cover therefore compensated for row orientation, and canopy cover influenced interrow position G_0 except when cover was nearly complete.

4. Conclusions

Discrepancies between calculated G_0 and calorimetric G_0 varied with respect to row orientation, canopy cover, and also depended on whether these were averaged across the interrow or partitioned into separate interrow sections. Overall discrepancy was least when both calculated G_0 and calorimetric G_0 were averaged across the interrow; i.e., positional variation was not considered. However, when interrow-average calculated G_0 was compared to shaded, partially sunlit, and fully sunlit interrow sections of calorimetric G_0, discrepancy was largest, especially for the NS row orientation with medium canopy cover. These discrepancies were reduced when calculated G_0 was also partitioned into shaded, partially sunlit, and fully sunlit interrow sections. It appears that accounting for positional variability as related to solar illumination is most justified for NS rows during sparse to medium canopy cover.

Discrepancy between calculated and calorimetric G_0 was larger for EW compared with NS rows. The larger discrepancy for the EW row orientation was at least partially related to volumetric soil water being measured at one depth and position (interrow center), whereas for the NS row orientation was measured at two depths and five positions spaced evenly across the interrow space. Although sensor accuracy used to measure volumetric soil water was addressed in other studies (Agam et al., 2012a; Evett et al., 2005), the relative model discrepancies for EW vs. NS rows may have also been partially related to use of capacitance vs. TDR probes, respectively.

For both NS and EW row orientations, discrepancy was largest during the BEG period (sparse canopy cover) and smallest during the END period (full canopy cover), where calculated $|G_{0,DAY}|$ > calorimetric $|G_{0,DAY}|$ resulted in negative MBE (up to -15.2 and -32.1 W m^{-2} for NS and EW, respectively) during the BEG period. This may have simply resulted from the magnitude of $G_{0,DAY}$ being larger during smaller canopy cover. In addition, it may have been related to errors in calculated $R_{N,S}$, the assumptions of $G_{0,MAX}=-R_{N,S,MIN}$ and $G_{0,MIN}=a\times R_{N,S,MAX}$ used in the normalized G_0 and normalized $R_{N,S}$ relation, and the assumption that the empirical value $a=-0.31$ remains constant throughout the crop growing season. Because $R_{N,S}$ measurements were not available in the present study, the relative contribution of the $R_{N,S}$ component to overall G_0 model discrepancy could not be assessed. Therefore, future studies of soil heat flux should strive to include measurements of $R_{N,S}$ and other relevant variables near the soil surface, along with accurate volumetric soil water measurements at appropriate spatial and temporal resolutions.

Acknowledgements

This research was supported by the USDA-ARS National Program 211, Water Availability and Watershed Management and in part by the Ogallala Aquifer Program, a consortium between USDA-Agricultural Research Service, Kansas State University, Texas AgriLife Research, Texas AgriLife Extension Service, Texas Tech University, and West Texas A&M University. We thank the numerous biological technicians and student workers for their meticulous and dedicated efforts in executing experiments and obtaining and processing data. The anonymous reviewer provided many helpful suggestions and comments, which improved the clarity of this manuscript.

References

Agam, N., Kustas, W.P., Evett, S.R., Colaizzi, P.D., Cosh, M., McKee, L.G., 2012a. Soil heat flux variability influenced by row direction in irrigated cotton. Adv. Water Resour. 50, 20–30.

Agam, N., Evett, S.R., Tolk, J.A., Kustas, W.P., Colaizzi, P.D., Alfieri, J.G., McKee, L.G., Copeland, K.S., Howell, T.A., Chávez, J.L., 2012b. Evaporative loss from irrigated interrows in a highly advective semi-arid agricultural area. Adv. Water Resour. 50, 20–30.

Allen, R.G., Periera, L.S., Raes, D., Smith, M., 1998. Crop evapotranspiration: guidelines for computing crop water requirements. In: Irrigation and Drainage Paper No. 56, Rome, Italy: United Nations FAO.

Colaizzi, P.D., Evett, S.R., Howell, T.A., Tolk, J.A., 2006. Comparison of five models to scale daily evapotranspiration from one-time-of-day measurements. Trans. ASABE 49 (5), 1409–1417.

Colaizzi, P.D., Evett, S.R., Howell, T.A., Li, F., Kustas, W.P., Anderson, M.C., 2012. Radiation model for row crops: I. Geometric model description and parameter optimization. Agron. J. 104 (2), 225–240.

Colaizzi, P.D., Agam, N., Tolk, J.A., Evett, S.R., Howell, T.A., Gowda, P.H., O'Shaughnessy, S.A., Kustas, W.P., Anderson, M.C., 2014. Two source energy balance model to calculate E, T, and ET: comparison of Priestley–Taylor and Penman–Monteith formulations and two time scaling methods. Trans. ASABE 57 (2), 479–498.

Colaizzi, P.D., Evett, S.R., Agam, N., Schwartz, R.C., Kustas, W.P., 2015. Soil heat flux calculation for sunlit and shaded surfaces under row crops: 1. Model development and sensitivity analysis. Agric. For. Meteorol., http://dx.doi.org/10.1016/j.agrformet.2015.10.010.

Cosh, M.H., Evett, S.R., McKee, L., 2012. Surface soil water content spatial organization within irrigated and non-irrigated agricultural fields. Adv. Water Resour. 50, 55–61.
Evett, S.R., 2000a. The TACQ program for automatic time domain reflectometry measurements: I. Design and operating characteristics. Trans. ASAE 43 (6), 1939-1946.
Evett, S.R., 2000b. The TACQ program for automatic time domain reflectometry measurements: II. Waveform interpretation methods. Trans. ASAE 43 (6), 1947–1956.
Evett, S.R., Tolk, J.A., Howell, T.A., 2005. TDR laboratory calibration in travel time, bulk electrical conductivity, and effective frequency. Vadose Zone J. 4, 1020–1029.
Evett, S.R., Agam, N., Kustas, W.P., Colaizzi, P.D., Schwartz, R.C., 2012a. Soil profile method for soil thermal diffusivity, conductivity, and heat flux: comparison to soil heat flux plates. Adv. Water Resour. 50, 41–54.
Evett, S.R., Kustas, W.P., Gowda, P.H., Anderson, M.C., Prueger, J.H., Howell, T.A., 2012b. Overview of the Bushland Evapotranspiration and Remote sensing EXperiment 2008 (BEAREX08): a field experiment evaluating methods for quantifying ET at multiple scales. Adv. Water Resour. 50, 4–19.
Ham, J.M., Kluitenberg, G.J., 1993. Positional variation in the soil energy balance beneath a row-crop canopy. Agric. For. Meteorol. 63, 73–92.
Heilman, J.L., McInnes, K.J., Savage, M.J., Gesch, R.W., Lascano, R.J., 1994. Soil and canopy energy balances in a west Texas vineyard. Agric. For. Meteorol. 71, 99–114.
Kustas, W.P., Daughtry, C.S.T., 1990. Estimation of the soil heat flux/net radiation ratio from spectral data. Agric. For. Meteorol. 49, 205–223.
Kustas, W.P., Daughtry, C.S.T., Van, P.J., Oevelen, 1993. Analytical treatment of the relationships between soil heat flux/net radiation ratio and vegetation indices. Remote Sens. Environ. 46, 319–330.
Kustas, W.P., Prueger, J.H., Hatfield, J.L., Ramalingam, K., Hipps, L.E., 2000. Variability in soil heat flux from a mesquite dune site. Agric. For. Meteorol. 103, 249–264.
Legates, D.R., McCabe Jr., G.J., 1999. Evaluating the use of "goodness-of-fit" measures in hydrologic and hydroclimatic model validation. Water Resour. Res. 35 (1), 233–241.
Maes, W.H., Steppe, K., 2012. Estimating evapotranspiration and drought stress with ground-based thermal remote sensing in agriculture: a review. J. Exp. Bot. 63 (13), 4671–4712, http://dx.doi.org/10.1093/jxb/ers165.
Nash, J.E., Sutcliffe, J.V., 1970. River flow forecasting through conceptual models part I – a discussion of principles. J. Hydrol. 10 (3), 282–290.
Peters, R.T., Evett, S.R., 2004. Modeling diurnal canopy temperature dynamics using one-time-of-day measurements and a reference temperature curve. Agron. J. 96 (6), 1553–1561.
Pieri, P., 2010. Modeling radiative balance in a row-crop canopy: row-soil surface net radiation partition. Ecol. Model. 221, 791–801.
Santanello Jr., J.A., Friedl, M.A., 2003. Diurnal covariation in soil heat flux and net radiation. J. Appl. Meteorol. 42 (6), 851–862.
Sauer, T.J., Horton, R., 2005. Soil heat flux. In: Hatfield, J.L., Baker, J.M. (Eds.), Micrometeorology in Agricultural Systems, Agronomy Monograph no. 47. American Society of Agronomy, Madison, WI, pp. 131–154.
Schneider, A.D., Howell, T.A., 2000. Surface runoff due to LEPA and spray irrigation of a slowly permeable soil. Trans. ASAE 43 (5), 1089–1095.
Tolk, J.A., Howell, T.A., Evett, S.R., 2006. Nighttime evapotranspiration from alfalfa and cotton in a semiarid climate. Agron. J. 98 (3), 730–736.
USDA-NRCS, 2015. Soil Survey TX375: Potter County, Texas. USDA Natural Resources Conservation Service, Washington, DC, Available at: http://websoilsurvey.nrcs.usda.gov. (accessed 04.08.15).
Van Niel, T.G., McVicar, T.R., Roderick, M.L., van Dijk, A.I.J.M., Renzullo, L.J., van Gorsel, E., 2011. Correcting for systematic error in satellite-derived latent heat flux due to assumptions in temporal scaling: assessment from flux tower observations. J. Hydrol. 409 (1–2), 140–148.
Van Niel, T.G., McVicar, T.R., Roderick, M.L., van Dijk, A.I.J.M., Beringer, J., Hutley, L.B., van Gorsel, E., 2012. Upscaling latent heat flux for thermal remote sensing studies: comparison of alternative approaches and correction of bias. J. Hydrol. 468–469, 35–46.